doi:10.3772/j.issn.1006-6748.2016.04.010

Measurements and analysis at 400MHz and 2600MHz in corridor radio channel①

Yin Xiaoyu (尹晓宇)②*, Zheng Guoxin*, Ding Qingfeng**, Wang Tao*, Qiao Yantao***
(* Key Laboratory of Specialty Fiber Optics and Optical Access Networks, Shanghai University, Shanghai 200072, P. R. China)
(** School of Electrical and Electronic Engineering, East China Jiaotong University, Nanchang 330013, P. R. China)
(*** Department of Computer and Information Science University of Michigan, Dearborn 48128, USA)

Abstract

A propagation measurement campaign was performed at the 10th floor corridor of Xingjian Building, Shanghai University, China. The channel was sounded by pseudo noise (PN) sequence at carrier frequencies of 400- and 2600-MHz respectively. In order to obtain large scale and small scale propagation characteristics in the corridor, the receiver was moved along the corridor every 1.02 meter to record the impulse response. More than 280,000 impulse responses were recorded in the campaign. This work first describes the principle of the measurement, and then how the recorded raw data are processed. The results show that path loss exponent is related to frequency. The relationship between the root-mean squared (RMS) delay spread and the T-R separation distance is analyzed. The RMS delay spread and the mean excess delay spread against path loss are also given, which explain why the 2600MHz RMS delay spread is larger than that of 400MHz.

Key words: path loss, root-mean squared (RMS) delay spread, corridor, channel measurement

0 Introduction

LTE (long term evolution), one of the key technologies for 4G wireless communication systems, has been put forward to support high data rates and large capacity gains. Corridor is an important wireless channel. The scenario of which is everywhere in the world. The corridor propagation channel has been studied for decades. However, to the best of our knowledge, numerous papers have investigated the propagation at 450MHz ~2GHz and 5GHz ~60GHz[1-8], while Refs[1,2] has been paid to that of 400MHz and 2600MHz in the corridor studied the path-loss exponents at 450MHz, 1.35GHz, 1.89GHz and 5GHz. All path-loss exponents in the LOS condition are below 2. Refs[3-8] studied small-scale multipath propagation. In Refs[3-7], RMS delay spread in the corridor was calculated. But only in Ref.[7] the relationship between RMS delay spread and T-R separation distance was analyzed, while the others just gave the RMS delay spread at some positions. In Ref.[8], the relationship between Ricean K-factor and T-R separation was given. Since the LTE system will be widely used, it is essential to investigate the propagation characteristics on these bands.

A measurement is carried out to the 400- and 2600-MHz radio channels on the 10th floor corridor of Xingjian Building, Shanghai university, China. The measured results are shown in this work. Measurements in the time domain are performed by sending PN sequence . After processing and analyzing the measured raw data, it is observed that the fluctuations of the received power is large when the receiver is near the transmitter, and the fluctuations decrease when the transceiver distance increases. The pathloss exponent shows a relation with frequency, that is higher frequency signals exhibit smaller path loss exponent. RMS delay spread increases with the path loss, and also increases with frequency.

The remainder of this paper is organized as follows. In Section 1, the measurement environment is described. In Section 2, experimental setup and measurement procedure are presented. In Section 3, the principle of PN correlation method for measuring the radio channel is given. Section 4 shows the measure-

① Supported by the National Natural Science Foundation of China (No. 61132003, 61171086, 61501186) and Shanghai Natural Science Foundation under Grant (No. 14ZR1415100).
② To whom correspondence should be addressed. E-mail: ytuyxy@163.com
Received on Oct. 9, 2015

ments and analysis results. The study is concluded in Section 5.

1 Measurement environments

The measurement campaign was carried out at the 10th floor of Xingjian Building, Shanghai University. The floor plan is shown in Fig. 1. The corridor is 81m long, 2.51m wide and 3.22m high. The south and north walls are made of hollow bricks. The surface of the wall has a layer of lime. The ceiling of the corridor is reinforced concrete. A layer of fiber plasterboard is suspended 0.6m down from the top. The floor is marble. The north and south of the corridor are offices and each one has a wooden door. In the middle of the corridor, a metallic door is in the north face. Both ends have a metallic door, which is the same as the middle one. Both doors at the ends are closed during the measurements campaign, but the middle one is open. A few metallic boxes are hanging on the wall. Nobody was moving around during the measurement campaign.

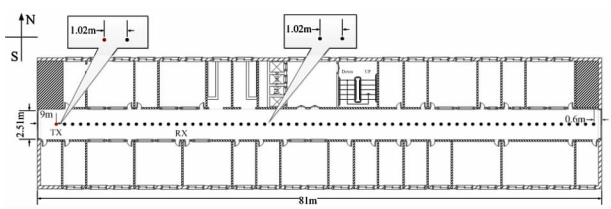

Fig. 1 Floor plan where the measurements are made

2 Experimental setup and measurement procedure

2.1 Experimental setup

A diagram of the measurement setup is shown in Fig. 2. The transmitter is an Agilent E8267D signal generator and the receiver is a R&S FSG8 frequency analyzer. The sounding signal PN sequence is generated by the signal generator. The bandwidth of the PN sequence is 50MHz. The sequence has 511 chips. The signal is modulated with carrier frequency of 400- and 2600-MHz. The modulated signal is transmitted through an omnidirectional antenna to the receiver.

The received signal is down-converted first and then digitized using an A/D converter with 100MHz sampling rate. The antennas are vertical polarization. The gain of the 400MHz antenna is 1dBi and the 2600MHz is 5dBi. Both of the antennas are omnidirectional antennas. The output power of the transmitter is 25dBm. A high-stability 10 MHz GPS reference clock provides high-frequency accuracy for both the transmitter and receiver.

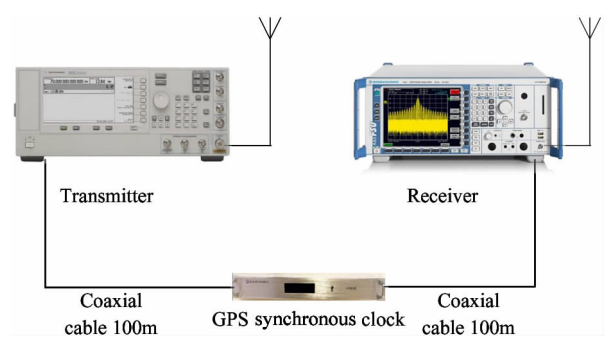

Fig. 2 Channel sounding setup

2.2 Measurement procedure

The transmitter is located at 9m away from the west end of the corridor. Both antennas are 174cm above the floor. During the measurement, the transmitter is put in the location of Tx, as shown in Fig. 1. The receiver was moved along the corridor at 70 different positions , each position spaced 1.02m apart (The marbles on the floor are $1.02 \times 1.02\text{m}^2$, so 1.02m is chosen as the spacing). The first Rx position is 2.04m apart from the transmitter. Both the transmitter and the receiver are kept still for each measurement. Nobody was moving around during the measurement campaign.

3 Measurement principles

PN sequence possesses excellent autocorrelation properties[9], as illustrated in Fig. 3, where T_c is the chip time width. So it can be used to measure the radio

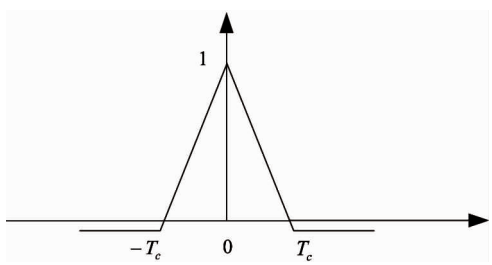

Fig. 3 Autocorrelation function of a PN sequence

channel. Assuming that $s(t)$ is the transmitted PN sequence, the received signal in the receiver will be

$$y(t) = s(t) \otimes h(t) = \int_{-\infty}^{\infty} s(\tau) h(t-\tau)\,\mathrm{d}\tau \quad (1)$$

where $\otimes$ denotes convolution, $h(t)$ is the channel impulse response(CIR) of the radio channel.

$$h(t,\tau) = \sum_{i=1}^{M} a_i \delta(t-\tau_i) \quad (2)$$

where M is the number of multipath components at the receiver, a_i and τ_i are the amplitude and delay shift of

the ith path respectively. $\delta(\cdot)$ is the delta function.

Cross-correlating $s(t)$ with $y(t)$, the following is obtained:

$$R(\tau) = \int_{-\infty}^{\infty} y(t)s(t-\tau)\mathrm{d}t \quad (3)$$

Exchange t and τ in Eq. (3)

$$\begin{aligned} R(t) &= \int_{-\infty}^{\infty} y(\tau)s(\tau-t)\mathrm{d}t \\ &= y(t) \otimes s(-t) \\ &= s(t) \otimes h(t) \otimes s(-t) \\ &= s(t) \otimes s(-t) \otimes h(t) \end{aligned} \quad (4)$$

From Eqs(3) and (4), it is obvious that the correlation of two signals is equal to the convolution of one signal's time reversal with the other signal. So $s(t) \otimes s(-t)$ is the autocorrelation function of $s(t)$, which is shown in Fig. 3. Then Eq. (4) is approximately equal

$$R(t) \approx \delta(t) \otimes h(t) = h(t) \quad (5)$$

It can be seen from above, correlation of the received signal with the original transmitted sequence directly yields the CIR.

If $s(t)$ is the transmitted PN sequence, the received signal results are

$$r(t) = \sum_{i=1}^{M} a_i s(t-\tau_i)(\cos(\omega_c t - \phi_i)) + n(t) \quad (6)$$

where $w_c/2\pi$ is the carrier frequency, M is the number of multipath components at the receiver, a_i, τ_i, ϕ_i are the amplitude, delay shift, phase shift of the ith path respectively and $n(t)$ is white Gaussian noise.

The received signal is down-converted to baseband IQ signal.

$$r_I(t) = \sum_{i=1}^{M} a_i s(t-\tau_i)\cos(\phi_i) \quad (7)$$

$$r_Q(t) = \sum_{i=1}^{M} a_i s(t-\tau_i)\sin(\phi_i) \quad (8)$$

Cross-correlating the coherently demodulated signals Eqs(7) and (8) with the template $s(t)$, the In-phase and Quadrature-phase components of the channel impulse response are obtained:

$$h_I(t) = \sum_{i=1}^{M} a_i R(t-\tau_i)\cos(\phi_i) \quad (9)$$

$$h_Q(t) = \sum_{i=1}^{M} a_i R(t-\tau_i)\sin(\phi_i) \quad (10)$$

$R(t)$ is the autocorrelation function of PN sequence $s(t)$.

The amplitude and phase of the ith path are Eq. (11) and Eq. (12), respectively.

$$a_i = \sqrt{h_I^2(\tau_i) + h_Q^2(\tau_i)} \quad (11)$$

$$\phi_i = \arctan\left(\frac{h_Q(\tau_i)}{h_I(\tau_i)}\right) \quad (12)$$

4 Measurement results and analysis

4.1 Large scale path loss

Using path loss models to design practical link budget is important for system analysis and design. Eq. (13) is the relationship between propagation path loss and T-R separation distance

$$PL(d)[dB] = \alpha + 10 \cdot \beta \log_{10}(d) + X_\sigma \quad (13)$$

where d is the T-R separation distance, α is the intercept in dB, β is the slope, and X_σ is a zero mean Gaussian random variable with a standard deviation σ in dB.

The values of α, β and σ are computed from the measured data, using linear regression such that the distance difference between the measured and estimated path losses is minimized in a mean square error.

A linear fit is made to the measured data; the fitted results are shown in Fig. 4 and Fig. 5 respectively. Coordinate - X is the logarithm of the T - R separation

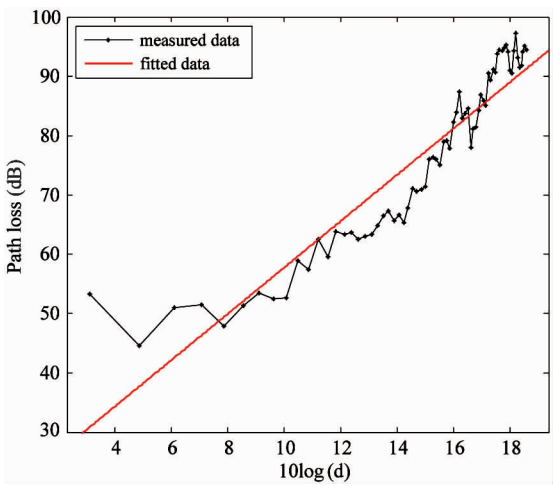

Fig. 4 400MHz path loss fitted results

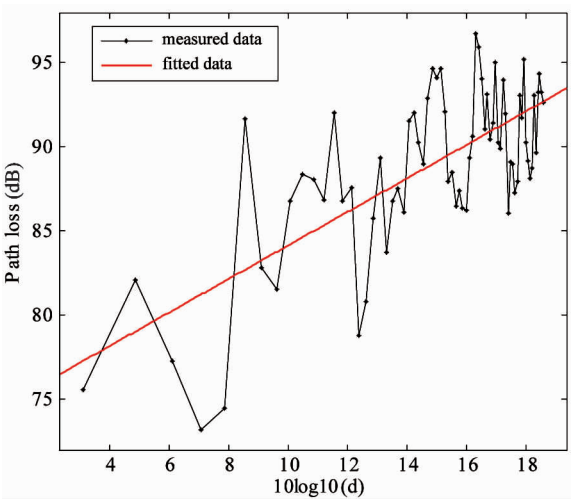

Fig. 5 2600MHz path loss fitted results

distance and coordinate-Y is the path loss attenuation in dB. Path loss exponent β is 3.901 and 0.993 for 400MHz and 2600MHz respectively. The standard deviation of 400MHz and 2600MHz are $\sigma_{400\text{MHz}} = 5.2589\text{dB}$ and $\sigma_{2600\text{MHz}} = 3.5649\text{dB}$ respectively.

The free space path loss model is given by

$$PL(dB) = -10\log_{10}\left[\frac{G_t G_r \lambda^2}{(4\pi)^2 d^2}\right] \tag{14}$$

where G_t is the transmitter antenna gain, G_r is the receiver antenna gain, λ is the wave length and d is the T-R separation distance.

Eq. (14) shows that under the same T-R separation, the lower the frequency, the smaller the path loss. From Fig. 4 and Fig. 5. It is seen that the 400MHz path loss is below that of 2600MHz in the short T-R separation distance, which is the same as free space. But the 400MHz path loss is greater than that of 2600MHz with the increase of T-R separation distance gradually. So the 400MHz path loss exponent is relatively large. From the measured data, it is observed that higher frequency causes smaller path loss exponent in the confined environment, which has the similar results with Ref. [10]. In Ref. [10] a large scale propagation measurement at carrier frequency of 450MHz and 900MHz in an arched tunnel of Massif Central in south-central France was performed. The tunnel is 3500m long, 7.8m wide, 5.3m high. The measured results show that the attenuation at 450MHz is larger than 900MHz.

The corridor can be considered as a rectangular waveguide surrounded by a lossy medium. So in the corridor the radio wave propagation involves many hybrid electromagnetic modes. Their attenuation constants are expressed as Eq. (55) in Ref. [10]. From the equation we know that the higher the frequency, the smaller the attention; the higher the mode, the larger the attention. In Fig. 4 and Fig. 5, the received power has a large fluctuation near the transmitter. This is because in the short T-R separation region, there are more higher order modes that cause large fluctuations, whereas in the long T-R separation region, higher modes have large attention, only the fundamental mode works, the fluctuation diminish in the region gradually. Comparing Fig. 4 with Fig. 5, the fluctuation of 2600MHz is a large than 400MHz. Higher frequency can cause much higher order mode, so 2600MHz has a large fluctuation.

4.2 Time dispersion

A weak signal will be submerged by noise. Signals are correlated, noises are uncorrelated. So use coherent integration can be used to enhance signal to noise ratio (SNR) if the channel is time-invariant. For the lower power path signal, it will be extracted from the noise.

Assuming that the signal power is σ_s, the noise power is σ_n, X_s is signal, $E(\cdot)$ is the expectation of $(\cdot)$. If N periods signals are added, then the total signals power is

$$\sigma_{s\text{-}all} = E\left(\left(\sum_{i=1}^{N}(X_s)_i\right)^2\right) = E((N\cdot X_s)^2) = N^2\cdot E(X_s^2) = N^2\cdot\sigma_s \tag{15}$$

Noises are uncorrelated, so the total noises power is

$$\sigma_{n\text{-}all} = E\left(\left(\sum_{i=1}^{N} n_i\right)^2\right) = N\cdot\sigma_n \tag{16}$$

where n_i is the ith period's noise.

After coherent integration, SNR is

$$SNR_{all} = \frac{N^2\sigma_s}{N\sigma_n} = N\frac{\sigma_s}{\sigma_n} = N\cdot SNR \tag{17}$$

SNR is the original. Process the measured data with coherent integration, SNR becomes N times of the original one. From Section 2, both IQ have 4103 frames. Process the 4103 frames measured data with coherent integration, the influence of noise can be reduced.

Power delay profile (PDP) of each position can be calculated using the raw data. Fig. 6 and Fig. 7 are the PDP of 400MHz and 2600MHz with T-R separation 37.74m.

The mean excess delay is the first moment of the PDP and is defined as

$$\bar{\tau} = \frac{\sum_k a_k^2\tau_k}{\sum_k a_k^2} = \frac{\sum_k p(\tau_k)\tau_k}{\sum_k p(\tau_k)} \tag{18}$$

The RMS delay spread is the square root of the second central moment of PDP and is defined as

$$\tau_{RMS} = \sqrt{\tau^2 - (\bar{\tau})^2} \tag{19}$$

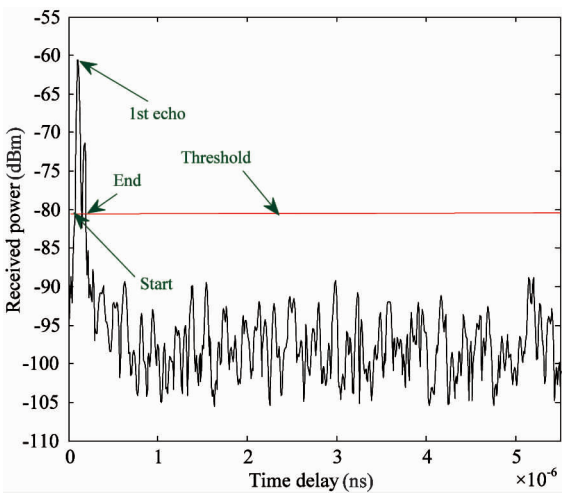

Fig. 6 400MHz PDP

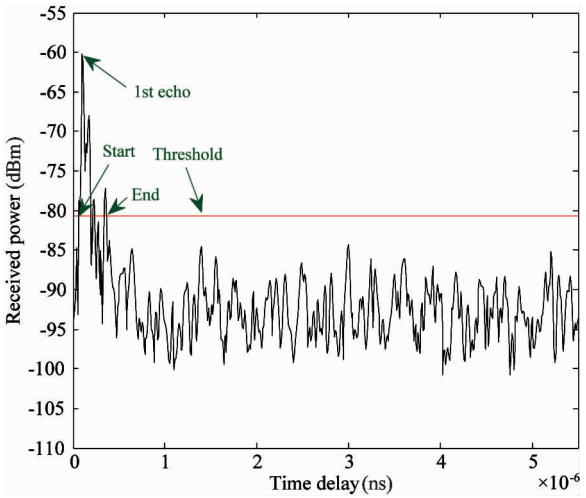

Fig. 7 2600MHz PDP

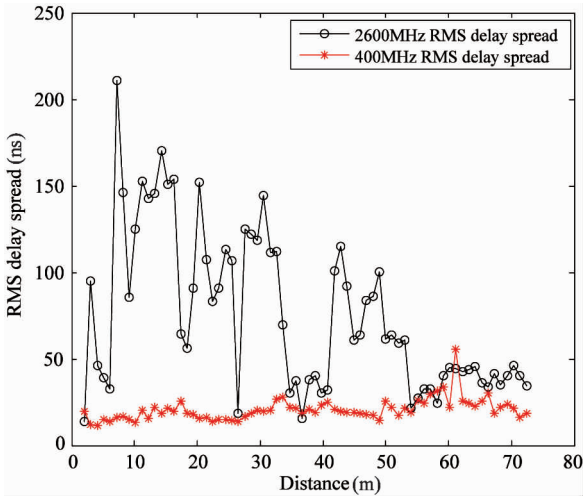

Fig. 8 RMS delay spread vs. T-R separation distance

where

$$\overline{\tau^2} = \frac{\sum_k a_k^2 \tau_k^2}{\sum_k a_k^2} = \frac{\sum_k p(\tau_k)\tau_k^2}{\sum_k p(\tau_k)} \tag{20}$$

In order to calculate the RMS delay spread, a threshold that 20dB below the peak value was chosen[11]. $\bar{\tau}$ in Eq. (2) is calculated according to Ref. [12]

$$\bar{\tau} = \frac{\sum_k p(\tau_k)\tau_k}{\sum_k p(\tau_k)} - \tau_A \tag{21}$$

where τ_A is the first arriving echo, $p(\tau_k)$ is the power above the threshold, τ_k is its delay, k is the kth samples of the PDP.

According to Eqs (18) ~ (21) and Fig. 6 and Fig. 7, RMS delay spread and mean excess delay spread are calculated.

Fig. 8 shows the RMS delay spread as a function of T-R separation distance. The 2600MHz RMS delay spread decreases as the T-R separation distance increases. The maximum value is 209ns, which is shown in the T-R separation distance of 7.14m. The 400MHz RMS delay spread increases first and then decreases. The maximum is shown in the T-R separation distance of 61.2m, and the value is 34.6ns. Fig. 9 shows the RMS delay spread CDF for 400MHz and 2600MHz. For 400MHz RMS delay spread it is apparent that most of delays arrive within 16ns; for 2600MHz, it is 61ns.

It is found that 2600MHz RMS delay spread is larger than 400MHz in the corridor. The RMS delay spread measured in papers is usually tens of nanoseconds[13].

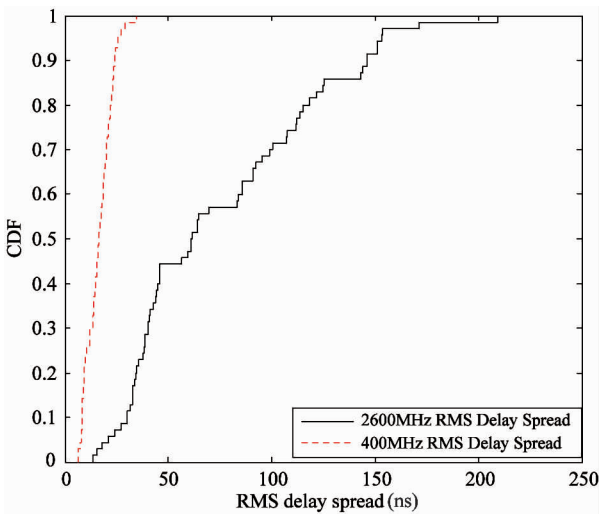

Fig. 9 2600MHz and 400MHz RMS delay spread CDF

It is found that large RMS delay spread is caused by the east metallic door at the end of the corridor. As the receiver move away from the transmitter, the distance difference between the direct signal propagation distance and the signal reflected from the metallic door becomes smaller. So the phenomenon in Fig. 8 appears in the 2600MHz RMS delay spread. But the path loss of 400MHz is so large that in the short distance of T-R separation the reflected signal can't reach the receiver. Until the T-R separation is about 60m, the receiver receives the reflected signal . So the 400MHz RMS delay spread increased first and then decreases.

Ref. [14] presented the exponential fits of RMS delay spread against path loss

$$\tau_{RMS} = \exp(aP_1 + b) \tag{22}$$

The coefficients for the different frequencies are given in Table 1 and the best fits are shown in Fig. 10 and Fig. 11.

Table 1 Coefficients of the exponential fit of RMS delay spread and path loss for different frequencies

Carrier frequency (MHz)	a	b
2600	0.01604	3.506
400	0.01702	1.514

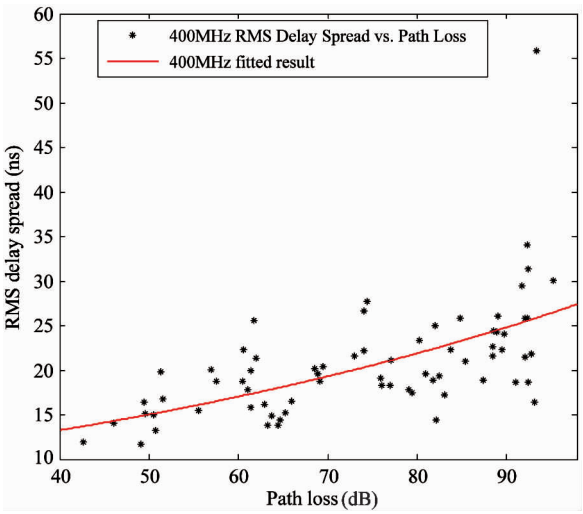

Fig. 10 400MHz RMS delay spread vs. path loss

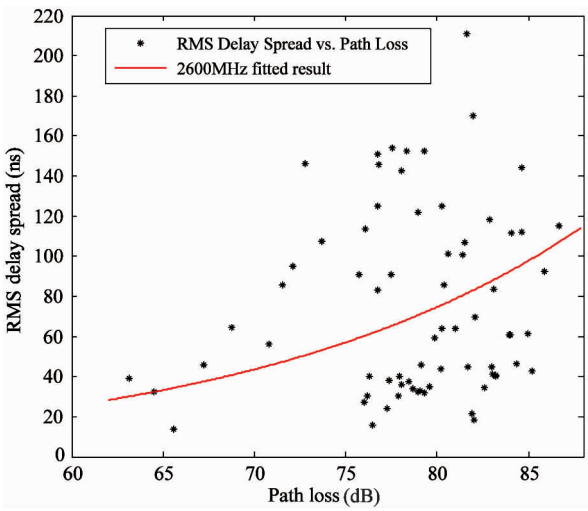

Fig. 11 2600MHz RMS delay spread vs. path loss

Comparing Fig. 8, Fig. 10 and Fig. 11, it is apparent that large RMS delay spread corresponds to high path loss.

Comparing RMS delay spread of 2600MHz with 400MHz, it is find that higher frequency causes larger RMS delay spread. It is the same as Ref. [15] expressed. Ref. [15] performed a measurement campaign in tunnel environment for 900MHz and 1800MHz. The RMS delay spread shows a strong relation with frequency. The measurements on average, 2600MHz RMS delay spread is 45ns larger than 400MHz.

Fig. 12 shows the exponential fits of mean excess delay spread against path loss. The mean excess delay spread against path loss was also fitted to an exponential, and best fit of the form of Eq. (23). The coefficients for the different frequency are given in Table 2:

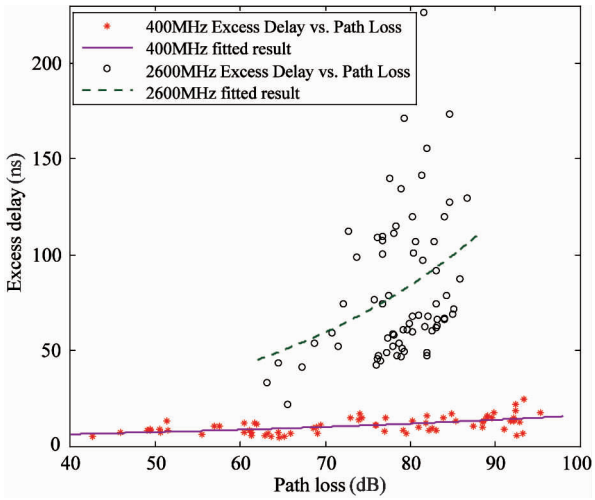

Fig. 12 Mean excess delay spread vs. path loss

Table 2 Coefficients of the exponential fit of mean excess delay and path loss for different frequencies

Carrier frequency (MHz)	a	b
2600	0.03439	1.678
400	0.01558	1.277

Another important time dispersion parameter is the ratio of τ_m/τ_{RMS}. τ_m is the mean excess delay spread and τ_{RMS} is the RMS delay spread. Indeed, lower values of the ratio indicate that a higher power level is concentrated at small values of the excess delay[16]. In Fig. 13, the ratio for 400MHz is smaller than 2600MHz. It is indicated that a higher power level is concentrated at smaller values of the excess delay at 400MHz than 2600MHz. The

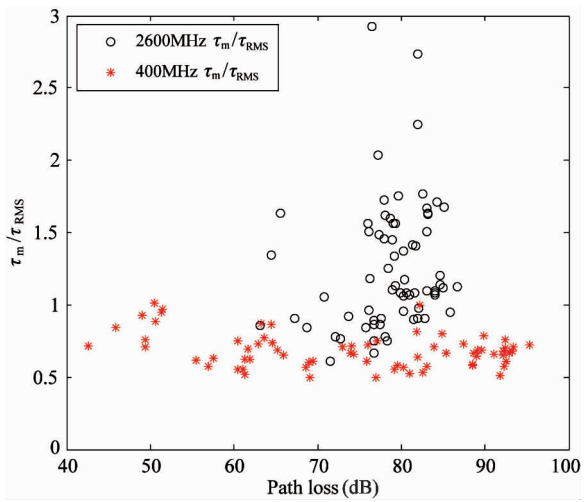

Fig. 13 τ_m/τ_{RMS} vs. path loss

receiver has a limited dynamic range. For 400MHz, large excess delay values has a low power, it cannot be detected. That is why 400MHz has a low RMS delay spread. But for 2600MHz, large excess delay has higher power, which can be detected by the receiver. 2600MHz has larger RMS delay spread.

5 Conclusions

A propagation measurement campaign at the 10th floor corridor of Xingjian Building, Shanghai University, China was performed. To measure the 400MHz and 2600MHz radio channels, PN sequence with 50MHz bandwidth was used. The transmitter is Agilent E8267D vector signal generator and the receiver is R&S FSG8 frequency analyzer. The sounding principle is described in detail. Coherent integration is used to process the raw data, which enhancs the SNR. PDP is used to calculate the RMS delay spread. The 2600MHz RMS delay spread as a function of T-R separation distance follows a downward trend as the T-R separation distance increases. The 400MHz RMS delay spread increases first and then decreases. Both the RMS and mean excess delay spread have an exponential relationship with path loss. The measurement is useful for LTE mobile communication in the corridor.

References

[1] Chandra A, Kumar A, aChandra P. Comparative study of path losses from propagation measurements at 450 MHz, 900 MHz, 1.35GHz and 1.89GHz in the corridors of a multifloor laboratory-cum-office building. In: Proceedings of the IEEE 50th Vehicular Technology Conference, Amsterdam, Netherlands, 1999. 2272-2276

[2] Zhao X, Geng S, Coulibaly B M. Path-loss model including LOS-NLOS transition regions for indoor corridors at 5GHz [Wireless Corner]. *IEEE Antennas and Propagation Magazine*, 2013, 55(3): 217-223

[3] Tan C A, Nix A R, Beach M A. Dynamic spatial-temporal propagation measurement and super-resolution channel characterization at 5.2 GHz in a corridor environment. In: Proceedings of the 56th IEEE Vehicular Technology Conference, Vancouver, Canada, 2002. 797-801

[4] Moraitis N, Constantinou P. Measurements and characterization of wideband indoor radio channel at 60GHz. *IEEE Transactions on Wireless Communications*, 2006, 5(4): 880-889

[5] Oestges C, Vanhoenacker-Janvier D, Clerckx B. Channel characterization of indoor wireless personal area networks. *IEEE Transactions on Antennas and Propagation*, 2006, 54(11):3143-3150

[6] Sheikh A U H, Mahmood M N. Channel sounding in corridors of an academic building. In: Proceedings of the 7th International Conference on Information, Communications and Signal Processing, Macau, China, 2009. 1-4

[7] Kivinen J, Vainikainen P. Wideband propagation measurements in corridors at 5.3GHz. In: Proceedings of the 5th IEEE International Symposium on Spread Spectrum Techniques and Applications, Sun City, South Africa, 1998. 512-516

[8] Wang Q, Ai B, Guan K, et al. Ray-based analysis of small-scale fading for indoor corridor scenarios at 15GHz. In: Proceedings of the Asia-Pacific Symposium on Electromagnetic Compatibility (APEMC), Taipei, China, 2015. 181-184

[9] Sarwate D V, Pursley M B. Cross correlation properties of pseudorandom and related sequences. *Proceedings of the IEEE*, 1980, 68(5):593-619

[10] Dudley D G, Lienard M, Mahmoud S F, et al. Wireless propagation in tunnels. *IEEE Antennas and Propagation Magazine*, 2007, 49(2):11-26

[11] Böttcher A, Schneider C, Vary P, et al. Dependency of the power and delay domain parameters on antenna height and distance in urban macro cell. In: Proceedings of the 5th European Conference on Antennas and Propagation (EUCAP), Rome, Italy, 2011. 1395-1399

[12] Cox D C, Leck R. Distributions of multipath delay spread and average excess delay for 910MHz urban mobile radio paths. *IEEE Transactions on Antennas and Propagation*, 1975, 23(2):206-213

[13] Rappaport T S. Wireless Communications: Principles and Practice. 2nd ed. Upper Saddle River, NJ, USA: Prentice-Hall, 2002. 199

[14] Salous S, Hinostroza V. Wideband indoor frequency agile channel sounder and measurements. *IEE Proceedings – Microwaves, Antennas and Propagation*, 2005, 152(6): 573-580

[15] Zhang Y P, Hwang Y. Characterization of UHF radio propagation channels in tunnel environments for microcellular and personal communications. *IEEE Transactions on Vehicular Technology*, 1998, 47(1):283-296

[16] Ciccognani W, Durantini A, Cassioli D. Time domain propagation measurements of the UWB indoor channel using PN-sequence in the FCC-compliant band 3.6-6 GHz. *IEEE Transactions on Antennas and Propagation*, 2005, 53(4):1542-1549

Yin Xiaoyu, born in 1988. He is a Ph. D candidate in School of Communication and Information Engineering, Shanghai University. His research interests include the confined environment wireless radio channel measurements and modeling.